

Fluidization and anomalous density fluctuations in epithelial tissues with pulsating activity

Zhu-Qin Li,¹ Qun-Li Lei,^{1,*} and Yu-qiang Ma^{1,†}

¹National Laboratory of Solid State Microstructures and School of Physics,
Collaborative Innovation Center of Advanced Microstructures, Nanjing University, 210093 Nanjing, China

Cells not only can have self-motility by crawling, but also are capable of other types of active motions like periodic contraction or pulsation. In this work, by using the Voronoi cell model, we show how this non-motility activity affects the structure, dynamic and density fluctuations of cellular monolayers. We found that random cell pulsation can fluidize solid epithelial tissues, resulting in a *hyperuniform* fluid state, while pulsation synchronization inhibits the fluidity, causes a reversed solidification. We prove this solidification is BKT-type transition, characterized by strong density/dynamic heterogeneity arising from the creation of topological defects in the pulsating phase space. The magnitude and length scale of density heterogeneity diverge as the pulsating period increases, resulting in an opposite *giant* density fluctuation. Our findings accord with recent experimental observations and can be quantitatively explained by a proposed fluctuating hydrodynamic theory.

Introduction Collective motions of cells in epithelial tissues play important roles in many vital life processes, like embryonic development, wound healing and cancer invasion [1–3], among which self-motility of cells was reported to induce solid-liquid (fluidization) transition [4–7], active turbulence or flocking [8–10] etc. [11–13]. On the other hand, non-motility activities, e.g., active cell deformation or periodic pulsation [14–17], also widely exist in cell tissues. For example, pulsating contractions induced by actin and myosin dynamics [18–31], which are closely related to contraction waves, morphogenesis and pattern formations in epithelial tissues [32–36]. Meanwhile, pulsating activity can also be caused by the exchange of fluid between cells gap junctions [37–39], or induced by active nuclear movements [40]. During these active pulsating processes, synchronization has been observed [23, 37]. How pulsating activities and their synchronization affect the fluidity of epithelial tissue still remains poorly understood. Moreover, epithelial tissue shows giant density fluctuations driven by collective cell migration or cell pulsation [37, 41], while in other cellular systems, hyperuniform states were reported [42–45]. Thus, it is also interesting to reveal the connection between non-motility activities and anomalous density fluctuations in epithelial tissues.

In this work, we focus on the effect of pulsating activity on the structure, dynamics and density fluctuations of epithelial monolayers. Based on the Voronoi cell model, we find that random cell pulsation fluidizes epithelial tissue, generating a *hyperuniform* fluid state [46–48]. When cell pulsations are synchronised, the fluid state is reversely solidified. This synchronization-induced solidification is a Berezinskii-Kosterlitz-Thouless (BKT) type transition. At the transition point, density and dynamic heterogeneity emerge due to the creation of topological defects in the pulsating phase space. Both the magnitude and length scale of the density heterogeneity diverge as the pulsating period increases to infinity, which results in an opposite

giant density fluctuation [49]. We generalize the underlying mechanism based on a fluctuating hydrodynamic theory and prove that the above phenomena is insensitive to the form of pulsation. Our findings provide a simple explanation for recently observed giant density fluctuations and associated topological defects in MDCK cell monolayer [22, 23, 37].

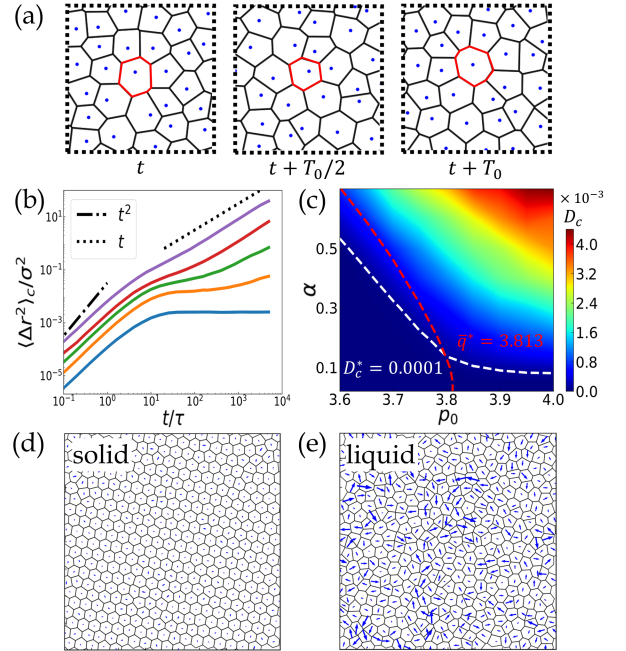


FIG. 1: (a) Schematics of a cell configuration (denoted in red) over a cell pulsating cycle T_0 . (b) MSD_c under different pulsating strength $\alpha = [0.1, 0.2, 0.3, 0.4, 0.7]$ (bottom to top). (c) Phase diagram of diffusion coefficient D_c . (d-e) Typical solid ($\rho_0 = 3.7, \alpha = 0.2$) and fluid ($\rho_0 = 3.7, \alpha = 0.6$) configurations. Blue arrows show the cell displacements after one period. All data are for random pulsation systems ($J = 0$) with $N = 400$.

Model We consider a 2D confluent cell monolayer composed of N pulsating cells whose area and shape can change with time (Fig. 1a). Cells are modelled as polygons determined by the Voronoi tessellation of the space [6]. We assume the pulsation is strong enough that the effect of thermal noise can be neglected. The center of cell i thus obeys the overdamped dynamics, i.e., $\dot{\mathbf{r}}_i = \mu \mathbf{F}_i$ with μ is the mobility coefficient and $\mathbf{F}_i = -\nabla_i E$ the inter-cellular force acting on particle i . The system energy E can be written as [6, 50–52]

$$\frac{E}{K_A A_0^2} = \sum_i^N [(a_i - a_0^i)^2 + \xi(p_i - p_0^i)^2]. \quad (1)$$

Here, $A_0 = L^2/N$ is the averaged cell area and K_A the area modulus of cell. a_i and p_i are the dimensionless area and perimeter of cell i , while the corresponding a_0^i and p_0^i are their targeted values. ξ is the dimensionless perimeter modulus. To model cell pulsation, we assume each a_0^i do stochastic oscillation as $a_0^i = 1 + \alpha \sin \varphi_i(t)$ where α is the pulsating strength and $\varphi_i(t)$ is the pulsating phase. $p_0^i = p_0$ with p_0 the so-called *target shape factor* [6]. To account for collective cell pulsation, we assume $\varphi_i(t)$ obeys the simple stochastic Kuramoto-like dynamics [53, 54] inspired from biological models [15, 16, 23, 24, 35], i.e.,

$$\frac{d\varphi_i}{dt} = \omega_0 + J \sum_{j \in C_i} \sin(\varphi_j - \varphi_i) + \sqrt{2T_\varphi} \eta_i(t). \quad (2)$$

where frequency ω_0 and the corresponding period $T_0 = 2\pi/\omega_0$ are supposed to be associated with certain intrinsic cell cycles [37]. The second term represents the coupling between adjacent cells with J the coupling strength. The last term is the noise term with noise strength T_φ and standard Gaussian white noise $\eta_i(t)$. In our simulation, the unit length, unit energy and unit time are defined as $\sigma = \sqrt{A_0}$, $\epsilon = K_A A_0^2$, $\tau = \sigma^2/\mu\epsilon$, respectively. We fixed $T_\varphi = 0.1\tau^{-1}$ and $T_0 = 200\tau$ if no state otherwise. Detail simulation information can be found in the Supplemental Material [55].

Cell-pulsation induced fluidization We first study the case of zero pulsation coupling ($J=0$). To accurately characterize the dynamical states of cellular monolayer, we calculate the cage relative mean square displacement of cells, $\text{MSD}_c(t)$, which excludes the influence of the long-wavelength fluctuations in 2D [8, 55]. As shown in Fig. 1b, with increasing α , the plateau of MSD_c gradually disappears and exhibits diffusion scaling. This indicates a pulsation-induced fluidization transition analogous to the one induced by motility [6]. Similar behaviors have been reported in the actively-deforming spherical particle system [14]. Microscopically, the fluidization transition is because random pulsation induces unbalanced intercellular forces, which results in frequent T1 transition (see Movie. S1 in [55]). In Fig. 1c, we plot the

diffusion coefficient D_c of the system in dimension of α and p_0 , where the solid and liquid phases are tentatively divided by a threshold $D_c^* = 10^{-4}\sigma^2/\tau$ [6]. We confirm that the solid phase in our model has the crystal order (see Movie. S2 and Fig. S1 in [55]). From Fig. 1c, one can see that systems with large p_0 are more easily fluidized as long as $\alpha \gtrsim 0.1$. This accords with the energy barrier scenario of T1 transition [5]. Nevertheless, by accurately calculating the average shape factor $\bar{q} = \sum_i (p_i/\sqrt{a_i})/N$, we find the line of zero-energy-barrier, i.e., $\bar{q}^* = 3.813$ [5, 6], does not correspond to the solid-liquid phase boundary determined by D_c^* , especially for small α . Similar discrepancy has also been observed experimentally [29].

Synchronization-induced solidification We further consider the intercellular coupling in the system. we find that increasing J leads to synchronization transition, which can be characterized by the phase polarity $M = \langle |\sum_i (\cos \varphi_i, \sin \varphi_i)| \rangle / N$. We plot M as a function of J and observe a transition happening at critical $J^* \simeq 0.06\tau^{-1}$ in Fig. 2a, which is almost invariant to the change of α and p_0 (see Fig. S2 in [55]). This is because the dynamic equation Eq. (2) for pulsating phase is formally decoupled from the energy function Eq. (1). Similar to the order-disorder transition in 2D XY model, 2D synchronization transition described by Kuramoto model belongs to BKT universality. In Fig. 2a, we plot the topological defect density $\rho_t = Q/N$ as a function of J and confirm that (de-)synchronization transition is indeed accompanied by the creation and annihilation of (± 1) topological defects in the pulsating phase space. In Fig. 2b, we further plot D_c in dimension of J and p_0 at fixed $\alpha=0.4$. We find that as J increases above J^* , D_c drops quickly, suggesting a synchronization-induced solidification. This collective phenomenon is insensitive to the choice of α and p_0 [55]. The reason behind this solidification is that compared with the unsynchronized state, the cell sizes in the synchronized state are more uniformly distributed [55]. Thus cells experience more balanced intercellular force during the collective pulsation, resulting in suppressed cell motions. This synchronization pulsation can capture the recently observed collective motions of the MDCK monolayer (see Movie. S3 in [55] and [36]).

In Fig. 2c, we give snapshots of the monolayer near the synchronization transition point. One can see the coexistence of high density contracted regions and low density expanded regions that periodically switch their states (see Movie. S4 in [55]). This density heterogeneity is strongest at J^* , as proven by the height of the first peak in structure factor $S(q)$ (Fig. 3c). In Fig. 2e, we also show that cell motility in the expanded regions is negligible like a solid, while in the contracted regions it is much higher akin to the liquid state. This dynamic heterogeneity is a result of heterogeneous distribution of local shape factor $\bar{q}_i(t) = (p_i(t)/\sqrt{a_i(t)})$ which is large (small) in the contracted (expanded) regions. A larger (smaller) shape

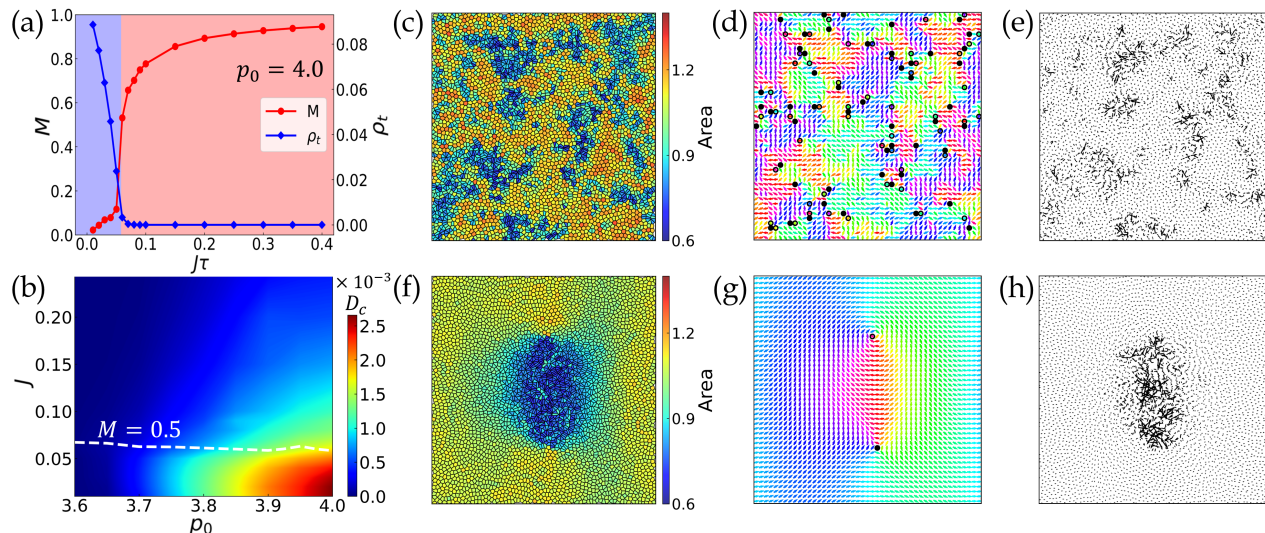


FIG. 2: (a) Phase polarization M (red line) and topological defect density ρ_t (blue line) as a function of J at fixed $p_0 = 4.0$, where the transition point is $J^* \simeq 0.06\tau^{-1}$. (b) Phase diagram of D_c at $\alpha = 0.4$. The white dashed line represents the synchronization transition points with $M = 0.5$. (c) Typical configuration of the system at $p_0 = 4.0$ and $J = 0.05\tau^{-1}$. The color indicates the size of cell area. (d) The pulsating phase field for the same configuration in (c) with the color arrow indicates the phase. The solid circle and open circle represents the $+1$ and -1 topological defects, respectively. (e) Instantaneous velocity field for the configuration in (c). (f-h) Cell configuration (f), pulsating phase field (g), and instantaneous velocity field (h), for a pair of topological defects at $p_0 = 4.0$, $J = 0.01\tau^{-1}$ and $T_\varphi = 0$. For all simulation, $N = 4096$.

factor corresponding to a more anisotropic (isotropic) cell shape and stronger (weaker) imbalanced intercellular forces which favour liquid (solid) phase [5, 6]. We notice that similar density heterogeneities and local synchronized pulsation patterns were observed in MDCK monolayers [20, 22, 37]. Furthermore, we plot the pulsating phase field of the cell monolayer near the critical point in Fig. 2d. We identify ± 1 topological defects and find they are mostly located on the boundaries between contracted and expanded regions. Surprisingly, these topological defects were also recently identified experimentally [23]. To further disclose the relationship between the topological defects and density/dynamic heterogeneities, we create a single pair of ± 1 topological defects in the phase field and observe its evolution (Fig. 2f-h). One can see that the topological defects create a synchronized cell droplet in between, which contracts (fluidizes) or expands (solidifies) alternatively. It also creates an local pulsating wave around the defect pair (see Movie. S5 in [55]). Thus, the synchronization-induced solidification of the monolayers is essentially a BKT-type transition, resulting from the annihilation of topological defects in the phase field.

Anomalous density fluctuations At last, we focus on the density fluctuations of the system. In Fig. 3a, we plot static structure factor $S(q)$ for random pulsation systems under different T_0 in the liquid state ($p_0 = 4.0$ and $\alpha = 0.4$). For systems with small T_0 , we observe $S(q \rightarrow 0) \sim q^2$, an hallmark of *hyperuniform* fluid state with vanishing density fluctuations at infinite wave length. Different from previously reported static hyperuniform states

in cellular systems [42–44], the hyperuniform fluid state here is dynamically robust to perturbation [47, 48]. With increasing T_0 , we find that the q^2 scaling remains unchanged, but the strength of hyperuniformity gradually decreases. Increasing α has similar effect (Fig. 3b). Thus the hyperuniformity is the strongest when cells undergo fast and weak pulsation in the liquid state.

With increasing J from zero to J^* , we find that a peak in $S(q)$ gradually develops around $q^* \sim 0.3 \sigma^{-1}$ without modifying q^2 scaling at small q regime (Fig. 3c). This indicates the coexistence of local large density fluctuations with global hyperuniformity, a scenario similar to circle swimmer systems [47]. Interestingly, with further increasing J , the height of first peak in $S(q)$ denoted as S_{max} gradually decreases. This is best shown in Fig. 3e, where we plot S_{max} as a function of J for two different p_0 . We find S_{max} exhibits diverging behavior when $J \rightarrow J^*$, which is more pronounced for large p_0 . In Fig. 3d, we further show $S(q)$ for various T_0 in synchronized states with $J = 0.4\tau^{-1}$. With increasing T_0 , S_{max} increases and the location of the peak q^* shifts to the small q . This indicates that both the magnitude and length scale of the density heterogeneity are controlled by T_0 , which diverge when $T_0 \rightarrow \infty$, resulting in *giant* density fluctuations (q^{-2} scaling). We find this mechanism is quite robust, independent whether the system is in solid or liquid phase (see Fig. S4 in [55]).

To understand the above anomalous density fluctuations, we construct a hydrodynamic theory based on cell

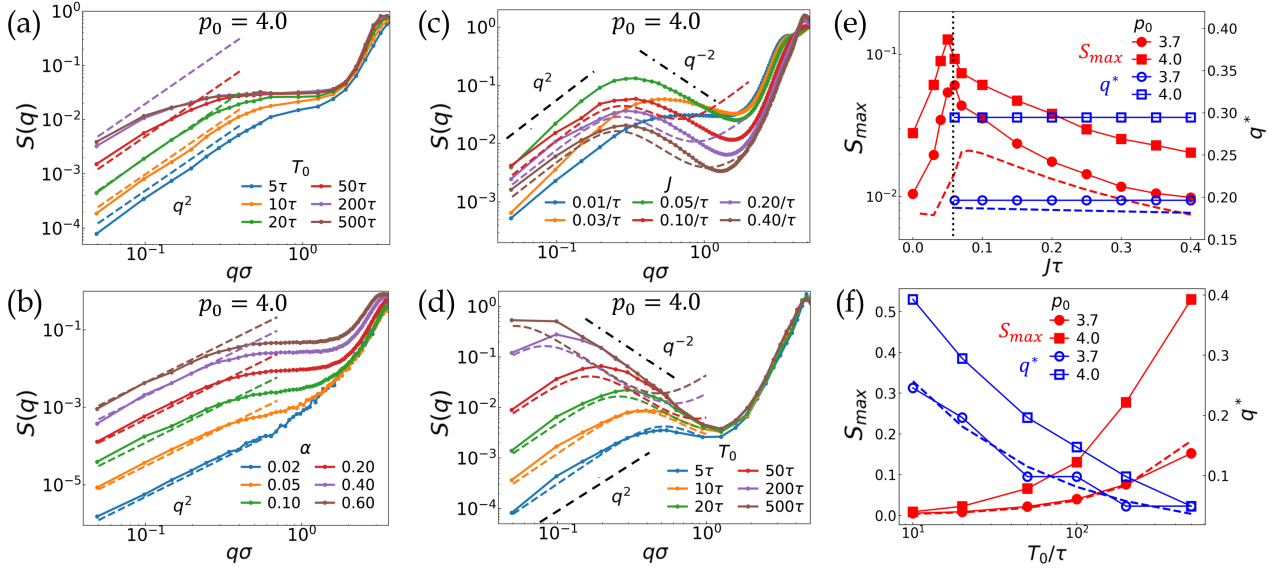


FIG. 3: (a-d) Simulation data (solid symbols) and theoretical predictions (dashed lines) of $S(q)$ for systems with: (a) different T_0 and fixed $(J, p_0, \alpha) = (0, 4.0, 0.4)$; (b) different α and fixed $(J, p_0, T_0) = (0, 4.0, 20\tau)$; (c) different J and fixed $(\alpha, p_0, T_0) = (0.4, 4.0, 20\tau)$; (d) different T_0 and fixed $(\alpha, p_0, J) = (0.4, 4.0, 0.4\tau^{-1})$. In (c) and (d), a correction $\chi = 0.25$ is used; (e-f) Simulation data of S_{max} (red solid symbols) and q^* (blue hollow symbols) as well as the corresponding theoretical predictions (dashed lines) for systems with: (e) different J and fixed $(\alpha, T_0) = (0.4, 20\tau)$; (f) different T_0 and fixed $(\alpha, J) = (0.4, 0.4\tau^{-1})$. Here, $N = 16384$ for all simulations. $\gamma = 1.1$ and simulation data of M are used for all theoretical predictions.

density field $\rho(\mathbf{r}, t)$ and pulsating phase field $\varphi(\mathbf{r}, t)$ [55],

$$\partial_t \rho = \frac{\mu}{\rho_0} \nabla \cdot (\rho \nabla P) + A_\alpha \nabla^2 \eta(\mathbf{r}, t). \quad (3)$$

$$\partial_t \varphi = \Omega + \sqrt{3} \frac{J}{\rho_0} \nabla^2 \varphi + \sqrt{2T_\varphi} \xi(\mathbf{r}, t). \quad (4)$$

where $P(\rho, \varphi) = -2K_A[\frac{1}{\rho} - \frac{1}{\rho_0}(1 + \alpha M \cos \varphi)] - K_P p_0^2(1 - \frac{\sqrt{\rho}}{\sqrt{\rho_0}})$ is the local pressure [55]. The second term in Eq. (3) is the center-of-mass conserved noise terms [47, 48, 56] caused by the active reciprocal interaction, i.e., cell pulsation. The strength of the noise is $A_\alpha = \gamma(1 - M)\alpha\sqrt{T_0}$ [55]. Eq. (4) is obtained by coarse-graining Eq. (2). η and ξ are two uncorrelated standard Gaussian white noise. From Eq. (3-4), we can obtain [55]

$$S(q) = 2T_\varphi \frac{\lambda_\alpha^2 (J' + D_\rho)}{J' D_\rho} \frac{q^2}{(J' + D_\rho)^2 q^4 + \Omega^2} + \frac{A_\alpha^2 q^2}{2D_\rho}. \quad (5)$$

The coefficients are $\lambda_\alpha = \frac{\alpha M \mu K_A}{\rho_0}$, $J' = \sqrt{3}J/\rho_0$, $D_\rho = \frac{\mu}{\rho_0}(\frac{2K_A}{\rho_0} + \frac{K_P p_0^2}{2})$, and $\Omega = 2\pi/T_0$. In the case of random pulsation ($M=0$ and $\lambda_\alpha=0$), $S(q)$ exhibits a q^2 hyperuniform scaling, as a result of the emergent long-range hydrodynamic correlation [48]. In Fig. 3a-b, we plot the theoretical prediction as the dashed line. We find the theory matches the simulation data well under different α and T_0 with only one adjustable parameter $\gamma=1.1$. In the case of synchronized state ($M=1$), the theory predicts the emerging of the first peak in $S(q)$ at finite T_0 and giant fluctuation q^{-2} scaling as $T_0 \rightarrow \infty$. In Fig. 3e-f, we plot the predicted height S_{max} and location of the first

peak q^* for the system as a function of J and T_0 , respectively. One can see that theoretical lines quantitatively match the simulation data without additional fitting parameter for the synchronized solid phase ($p_0=3.7$). Especially, the theory predicts a diffusion scaling relationship between the length scale of density heterogeneity and pulsating period, i.e., $q^{*-2} \simeq (J' + D_\rho)T_0$. For the liquid phase, due to large cell deformation, a correction $\chi(p_0)$ is needed in $D_\rho = \frac{\mu}{\rho_0}[\frac{2K_A}{\rho_0} + \chi(p_0)\frac{K_P p_0^2}{2}]$ to obtain the good fitting (Fig. 3c-d). The above fluctuating hydrodynamic theory indicates that the active reciprocal interaction and the competition of time scales between pulsation and stress relaxation are two key factors determining anomalous density fluctuations in the system.

Generalization to other pulsation form Our above modelling of cell pulsation is based on the stochastic oscillation of a_0^i . Biologically, cell pulsation might also come from time-dependent junction tension [21, 26–30]. Thus, we extend our studies to the case where p_0^i do stochastic oscillation as $p_0^i = p_0[1 + \beta \cos \varphi_i(t)]$ while $a_0^i = 1$. Here β represents the pulsating strength. We find similar hyperuniform fluid states at large β and synchronization-induced dynamical slowdown at large pulsating period (see Fig. S5-S7 in [55]). The hydrodynamic theory can also be extended to this pulsating scenario and obtain similar predictions [55]. All these results demonstrate the robustness of pulsating activity in determining the fluidization and anomalous density fluctuations in epithelial tissue.

Conclusion and discussion In this work, we show that random cell pulsation acting as reciprocal active force, melts solid epithelial tissues into hyperuniform fluids, while pulsating synchronization induces a reverse solidification. We prove that this solidification is BKT-type and the creation of topological defects in the pulsating phase space induces strong dynamical and structural heterogeneities at the transition point. Our findings can explain recent observed giant density fluctuations and topological defects in the MDCK monolayer [20, 22, 23, 37]. In the future, it is tempting to study the fluctuating physics of systems with complex couplings between pulsating phase and the motion of cells [15, 23], or pulsating cellular systems with nematic order [57–59]. Such exploration would help us understand how squeezing and contraction forces sculpt cell tissues [60–62] and guide the design of soft robot swarms [63].

Acknowledgments: The authors thank Ran Ni, Xia-qing Shi, Yan-Wei Li for careful reading the manuscript and helpful discussion, and are grateful to the High-Performance Computing Center of Collaborative Innovation Center of Advanced Microstructures, the High-Performance Computing Center (HPCC) of Nanjing University for the numerical calculations. This work is supported by the National Key Research and Development Program of China (No. 2022YFA1405000) and the National Natural Science Foundation of China (No. 12275127, 11974175, 12174184, and 12247102).

* Electronic address: lql@nju.edu.cn

† Electronic address: myqiang@nju.edu.cn

- [1] Friedl, P. & Gilmour, D. Collective cell migration in morphogenesis, regeneration and cancer. *Nature reviews Molecular cell biology* **10**, 445–457 (2009).
- [2] Hakim, V. & Silberzan, P. Collective cell migration: a physics perspective. *Reports on Progress in Physics* **80**, 076601 (2017).
- [3] Alert, R. & Trepat, X. Physical models of collective cell migration. *Annual Review of Condensed Matter Physics* **11**, 77–101 (2020).
- [4] Park, J.-A. *et al.* Unjamming and cell shape in the asthmatic airway epithelium. *Nature materials* **14**, 1040–1048 (2015).
- [5] Bi, D., Lopez, J., Schwarz, J. M. & Manning, M. L. A density-independent rigidity transition in biological tissues. *Nature Physics* **11**, 1074–1079 (2015).
- [6] Bi, D., Yang, X., Marchetti, M. C. & Manning, M. L. Motility-driven glass and jamming transitions in biological tissues. *Physical Review X* **6**, 021011 (2016).
- [7] Mongera, A. *et al.* A fluid-to-solid jamming transition underlies vertebrate body axis elongation. *Nature* **561**, 401–405 (2018).
- [8] Lin, S.-Z., Ye, S., Xu, G.-K., Li, B. & Feng, X.-Q. Dynamic migration modes of collective cells. *Biophysical journal* **115**, 1826–1835 (2018).
- [9] Giavazzi, F. *et al.* Flocking transitions in confluent tissues. *Soft matter* **14**, 3471–3477 (2018).
- [10] Cai, L.-b., Ji, W., Luo, J., Lei, Q.-l. & Ma, Y.-q. Numerical study of dynamic zigzag patterns in migrating epithelial tissue. *Science China Physics, Mechanics & Astronomy* **65**, 217011 (2022).
- [11] Petrolli, V. *et al.* Confinement-induced transition between wavelike collective cell migration modes. *Physical review letters* **122**, 168101 (2019).
- [12] Peyret, G. *et al.* Sustained oscillations of epithelial cell sheets. *Biophysical journal* **117**, 464–478 (2019).
- [13] Yu, J. *et al.* Spatiotemporal oscillation in confined epithelial motion upon fluid-to-solid transition. *ACS nano* **15**, 7618–7627 (2021).
- [14] Tjhung, E. & Berthier, L. Discontinuous fluidization transition in time-correlated assemblies of actively deforming particles. *Physical Review E* **96**, 050601 (2017).
- [15] Zhang, Y. & Fodor, É. Pulsating Active Matter. *Physical Review Letters* **131**, 238302 (2023).
- [16] Manacorda, A. & Fodor, É. Pulsating with discrete symmetry. *arXiv preprint arXiv:2310.14370* (2023).
- [17] Manning, M. L. Essay: Collections of deformable particles present exciting challenges for soft matter and biological physics. *Physical Review Letters* **130**, 130002 (2023).
- [18] Banerjee, S., Utuje, K. J. & Marchetti, M. C. Propagating stress waves during epithelial expansion. *Physical review letters* **114**, 228101 (2015).
- [19] Lin, S.-Z., Li, B., Lan, G. & Feng, X.-Q. Activation and synchronization of the oscillatory morphodynamics in multicellular monolayer. *Proceedings of the National Academy of Sciences* **114**, 8157–8162 (2017).
- [20] Hino, N. *et al.* ERK-mediated mechanochemical waves direct collective cell polarization. *Developmental cell* **53**, 646–660 (2020).
- [21] Krajnc, M., Stern, T. & Zankoc, C. Active instability and nonlinear dynamics of cell-cell junctions. *Physical Review Letters* **127**, 198103 (2021).
- [22] Boockock, D., Hino, N., Ruzickova, N., Hirashima, T. & Hannezo, E. Theory of mechanochemical patterning and optimal migration in cell monolayers. *Nature physics* **17**, 267–274 (2021).
- [23] Boockock, D., Hirashima, T. & Hannezo, E. Interplay between mechanochemical patterning and glassy dynamics in cellular monolayers. *bioRxiv* 2023–03 (2023).
- [24] Pérez-Verdugo, F., Banks, S. & Banerjee, S. Excitable dynamics driven by mechanical feedback in biological tissues. *arXiv preprint arXiv:2310.04950* (2023).
- [25] Pérez-Verdugo, F. & Banerjee, S. Tension Remodeling Regulates Topological Transitions in Epithelial Tissues. *PRX Life* **1**, 023006 (2023).
- [26] Dierkes, K., Sumi, A., Solon, J. & Salbreux, G. Spontaneous oscillations of elastic contractile materials with turnover. *Physical review letters* **113**, 148102 (2014).
- [27] Curran, S. *et al.* Myosin II controls junction fluctuations to guide epithelial tissue ordering. *Developmental cell* **43**, 480–492 (2017).
- [28] Krajnc, M. Solid–fluid transition and cell sorting in epithelia with junctional tension fluctuations. *Soft Matter* **16**, 3209–3215 (2020).
- [29] Devany, J., Sussman, D. M., Yamamoto, T., Manning, M. L. & Gardel, M. L. Cell cycle–dependent active stress drives epithelia remodeling. *Proceedings of the National*

- Academy of Sciences* **118**, e1917853118 (2021).
- [30] Yamamoto, T., Sussman, D. M., Shibata, T. & Manning, M. L. Non-monotonic fluidization generated by fluctuating edge tensions in confluent tissues. *Soft Matter* **18**, 2168–2175 (2022).
- [31] Duclut, C., Paijmans, J., Inamdar, M. M., Modes, C. D. & Jülicher, F. Active T1 transitions in cellular networks. *The European Physical Journal E* **45**, 29 (2022).
- [32] Solon, J., Kaya-Copur, A., Colombelli, J. & Brunner, D. Pulsed forces timed by a ratchet-like mechanism drive directed tissue movement during dorsal closure. *Cell* **137**, 1331–1342 (2009).
- [33] Martin, A. C., Kaschube, M. & Wieschaus, E. F. Pulsed contractions of an actin–myosin network drive apical constriction. *Nature* **457**, 495–499 (2009).
- [34] Armon, S., Bull, M. S., Aranda-Diaz, A. & Prakash, M. Ultrafast epithelial contractions provide insights into contraction speed limits and tissue integrity. *Proceedings of the National Academy of Sciences* **115**, E10333–E10341 (2018).
- [35] Staddon, M. F., Munro, E. M. & Banerjee, S. Pulsatile contractions and pattern formation in excitable actomyosin cortex. *PLoS Computational Biology* **18**, e1009981 (2022).
- [36] Thiagarajan, R., Bhat, A., Salbreux, G., Inamdar, M. M. & Riveline, D. Pulsations and flows in tissues as two collective dynamics with simple cellular rules. *IScience* **25** (2022).
- [37] Zehnder, S. M., Suaris, M., Bellaire, M. M. & Angelini, T. E. Cell volume fluctuations in MDCK monolayers. *Biophysical journal* **108**, 247–250 (2015).
- [38] Zehnder, S. M. *et al.* Multicellular density fluctuations in epithelial monolayers. *Physical Review E* **92**, 032729 (2015).
- [39] Zehnder, S. M., Zegers, F. M. & Angelini, T. E. A Langevin model of physical forces in cell volume fluctuations. *Journal of biomechanics* **49**, 1286–1289 (2016).
- [40] Bocanegra-Moreno, L., Singh, A., Hannezo, E., Zagorski, M. & Kicheva, A. Cell cycle dynamics control fluidity of the developing mouse neuroepithelium. *Nature Physics* 1–9 (2023).
- [41] Giavazzi, F. *et al.* Giant fluctuations and structural effects in a flocking epithelium. *Journal of Physics D: Applied Physics* **50**, 384003 (2017).
- [42] Jiao, Y. *et al.* Avian photoreceptor patterns represent a disordered hyperuniform solution to a multiscale packing problem. *Physical Review E* **89**, 022721 (2014).
- [43] Li, X., Das, A. & Bi, D. Biological tissue-inspired tunable photonic fluid. *Proceedings of the National Academy of Sciences* **115**, 6650–6655 (2018).
- [44] Zheng, Y., Li, Y.-W. & Ciamarra, M. P. Hyperuniformity and density fluctuations at a rigidity transition in a model of biological tissues. *Soft Matter* **16**, 5942–5950 (2020).
- [45] Liu, Y., Chen, D., Jiao, Y. & Tian, J. Universal Hyperuniform Organization of Cellular Structures in Leaf Vein Networks. *arXiv preprint arXiv:2311.09551* (2023).
- [46] Torquato, S. Hyperuniform states of matter. *Physics Reports* **745**, 1–95 (2018).
- [47] Lei, Q.-L., Ciamarra, M. P. & Ni, R. Nonequilibrium strongly hyperuniform fluids of circle active particles with large local density fluctuations. *Science advances* **5**, eaau7423 (2019).
- [48] Lei, Q.-L. & Ni, R. Hydrodynamics of random-organizing hyperuniform fluids. *Proceedings of the National Academy of Sciences* **116**, 22983–22989 (2019).
- [49] Shi, X.-q. & Ma, Y.-q. Topological structure dynamics revealing collective evolution in active nematics. *Nature communications* **4**, 3013 (2013).
- [50] Fletcher, A. G., Osterfield, M., Baker, R. E. & Shvartsman, S. Y. Vertex models of epithelial morphogenesis. *Biophysical journal* **106**, 2291–2304 (2014).
- [51] Alt, S., Ganguly, P. & Salbreux, G. Vertex models: from cell mechanics to tissue morphogenesis. *Philosophical Transactions of the Royal Society B: Biological Sciences* **372**, 20150520 (2017).
- [52] Li, X., Das, A. & Bi, D. Mechanical heterogeneity in tissues promotes rigidity and controls cellular invasion. *Physical review letters* **123**, 058101 (2019).
- [53] Acebrón, J. A., Bonilla, L. L., Vicente, C. J. P., Ritort, F. & Spigler, R. The Kuramoto model: A simple paradigm for synchronization phenomena. *Reviews of modern physics* **77**, 137 (2005).
- [54] Sarkar, M. & Gupte, N. Phase synchronization in the two-dimensional kuramoto model: Vortices and duality. *Physical Review E* **103**, 032204 (2021).
- [55] See Supplemental Material at [URL] for methods, supplementary datas, movies and complete hydrodynamic theory, which includes Refs. [36, 64–69] (????).
- [56] Hexner, D. & Levine, D. Noise, diffusion, and hyperuniformity. *Physical review letters* **118**, 020601 (2017).
- [57] Saw, T. B. *et al.* Topological defects in epithelia govern cell death and extrusion. *Nature* **544**, 212–216 (2017).
- [58] Zhang, G. & Yeomans, J. M. Active forces in confluent cell monolayers. *Physical Review Letters* **130**, 038202 (2023).
- [59] Rozman, J., Yeomans, J. M. & Sknepnek, R. Shapetension coupling produces nematic order in an epithelium vertex model. *Physical Review Letters* **131**, 228301 (2023).
- [60] Heisenberg, C.-P. & Bellaïche, Y. Forces in tissue morphogenesis and patterning. *Cell* **153**, 948–962 (2013).
- [61] Dance, A. The secret forces that squeeze and pull life into shape. *Nature* **589**, 186–189 (2021).
- [62] Bailles, A., Gehrels, E. W. & Lecuit, T. Mechanochemical principles of spatial and temporal patterns in cells and tissues. *Annual review of cell and developmental biology* **38**, 321–347 (2022).
- [63] Li, S. *et al.* Particle robotics based on statistical mechanics of loosely coupled components. *Nature* **567**, 361–365 (2019).
- [64] Fabri, A. & Pion, S. CGAL: The computational geometry algorithms library. In *Proceedings of the 17th ACM SIGSPATIAL international conference on advances in geographic information systems*, 538–539 (2009).
- [65] Li, Y.-W. & Ciamarra, M. P. Role of cell deformability in the two-dimensional melting of biological tissues. *Physical Review Materials* **2**, 045602 (2018).
- [66] Pasupalak, A., Yan-Wei, L., Ni, R. & Ciamarra, M. P. Hexatic phase in a model of active biological tissues. *Soft matter* **16**, 3914–3920 (2020).
- [67] Killeen, A., Bertrand, T. & Lee, C. F. Polar fluctuations lead to extensile nematic behavior in confluent tissues. *Physical Review Letters* **128**, 078001 (2022).
- [68] Rouzair, Y. & Levis, D. Defect superdiffusion and unbinding in a 2D XY model of self-driven rotors. *Physical Review Letters* **127**, 088004 (2021).
- [69] Shi, X.-q. & Chaté, H. Effect of Persistent Noise on the XY Model and Two-Dimensional Crystals. *arXiv*

preprint arXiv:2401.11175 (2024).